Investigation of optical absorptance of one-dimensionally periodic silicon gratings as solar absorbers for solar cells

Nghia Nguyen-Huu,[1,2,*] Michael Cada,[1] and Jaromír Pištora[2]

[1]*Department of Electrical and Computer Engineering, Dalhousie University, Halifax, Nova Scotia B3J 2X4, Canada*
[2]*Nanotechnology Centre, VSB Technical University of Ostrava, Ostrava-Poruba 708 33, Czech Republic*
[*]*nghianano@gmail.com*

Abstract: A rigorous design using periodic silicon (Si) gratings as absorbers for solar cells in visible and near-infrared regions is numerically presented. The structure consists of a subwavelength Si grating layer on top of an Si substrate. Ranges of grating dimensions are preliminary considered satisfying simple and feasible fabrication techniques with an aspect ratio defined as the ratio of the grating thickness (d) and the grating lamella width (w), with $0 < d/w < 1.0$. The subwavelength grating structure (SGS) is assumed to comprise different lamella widths and slits within each period in order to finely tune the grating profile such that the absorptance is significantly enhanced in the whole wavelength region. The results showed that the compound SGS yields an average absorptance of 0.92 which is 1.5 larger than that of the Si plain and conventional grating structures. It is shown that the absorptance spectrum of the proposed SGS is insensitive to the angle of incidence of the incoming light. The absorptance enhancement is also investigated by computing magnetic field, energy density, and Poynting vector distributions. The results presented in this study show that the proposed method based on nanofabrication techniques provides a simple and promising solution to design solar energy absorbers or other energy harvesting devices.

OCIS codes: (040.6040) Silicon; (050.2770) Gratings; (310.6628) Subwavelength structures, nanostructures; (350.6050) Solar energy.

References and links

1. H. Sai, Y. Kanamori, and H. Yugami, "High-temperature resistive surface grating for spectral control of thermal radiation," Appl. Phys. Lett. **82**(11), 1685–1687 (2003).
2. S. Y. Lin, J. Moreno, and J. G. Fleming, "Three-dimensional photonic-crystal emitter for thermal photovoltaic power generation," Appl. Phys. Lett. **83**(2), 380–382 (2003).
3. N. Nguyen-Huu, Y.-B. Chen, and Y.-L. Lo, "Development of a polarization-Insensitive thermophotovoltaic emitter with a binary grating," Opt. Express **20**(6), 5882–5890 (2012).
4. H. Sai, Y. Kanamori, K. Hane, and H. Yugami, "Numerical study on spectral properties of tungsten one-dimensional surface-relief gratings for spectrally selective devices," J. Opt. Soc. Am. A **22**(9), 1805–1813 (2005).
5. S. E. Han, A. Stein, and D. J. Norris, "Tailoring self-assembled metallic photonic crystals for modified thermal emission," Phys. Rev. Lett. **99**(5), 053906 (2007).
6. T. Asano, K. Mochizuki, M. Yamaguchi, M. Chaminda, and S. Noda, "Spectrally selective thermal radiation based on intersubband transitions and photonic crystals," Opt. Express **17**(21), 19190–19203 (2009).
7. S. E. Han and G. Chen, "Optical absorption enhancement in silicon nanohole arrays for solar photovoltaics," Nano Lett. **10**(3), 1012–1015 (2010).
8. N. P. Sergeant, M. Agrawal, and P. Peumans, "High performance solar-selective absorbers using coated sub-wavelength gratings," Opt. Express **18**(6), 5525–5540 (2010).
9. N. Nguyen-Huu and Y.-L. Lo, "Control of infrared spectral absorptance with one-dimensional subwavelength gratings," J. Lightwave Technol. **31**(15), 2482–2490 (2013).
10. R. Dewan, M. Marinkovic, R. Noriega, S. Phadke, A. Salleo, and D. Knipp, "Light trapping in thin-film silicon solar cells with submicron surface texture," Opt. Express **17**(25), 23058–23065 (2009).
11. J. G. Mutitu, S. Shi, C. Chen, T. Creazzo, A. Barnett, C. Honsberg, and D. W. Prather, "Thin film solar cell design based on photonic crystal and diffractive grating structures," Opt. Express **16**(19), 15238–15248 (2008).

#195307 - $15.00 USD Received 5 Aug 2013; revised 22 Oct 2013; accepted 25 Nov 2013; published 4 Dec 2013

12. I. Massiot, C. Colin, C. Sauvan, P. Lalanne, P. R. I. Cabarrocas, J.-L. Pelouard, and S. Collin, "Multi-resonant absorption in ultra-thin silicon solar cells with metallic nanowires," Opt. Express **21**(S3 Suppl 3), A372–A381 (2013).
13. R. Chriki, A. Yanai, J. Shappir, and U. Levy, "Enhanced efficiency of thin film solar cells using a shifted dual grating plasmonic structure," Opt. Express **21**(S3 Suppl 3), A382–A391 (2013).
14. S. Hava and M. Auslender, "Design and analysis of low-reflection grating microstructures for a solar energy absorber," Sol. Energ. Mat. Sol. **61**(2), 143–151 (2000).
15. A. Lin and J. Phillips, "Optimization of random diffraction gratings in thin-film solar cells using genetic algorithms," Sol. Energ. Mat. Sol. **92**(12), 1689–1696 (2008).
16. S. B. Mallick, M. Agrawal, and P. Peumans, "Optimal light trapping in ultra-thin photonic crystal crystalline silicon solar cells," Opt. Express **18**(6), 5691–5706 (2010).
17. C. S. Schuster, P. Kowalczewski, E. R. Martins, M. Patrini, M. G. Scullion, M. Liscidini, L. Lewis, C. Reardon, L. C. Andreani, and T. F. Krauss, "Dual gratings for enhanced light trapping in thin-film solar cells by a layer-transfer technique," Opt. Express **21**(S3 Suppl 3), A433–A439 (2013).
18. A. Bozzola, M. Liscidini, and L. C. Andreani, "Photonic light-trapping versus Lambertian limits in thin film silicon solar cells with 1D and 2D periodic patterns," Opt. Express **20**(S2 Suppl 2), A224–A244 (2012).
19. J. Zhu, C.-M. Hsu, Z. Yu, S. Fan, and Y. Cui, "Nanodome solar cells with efficient light management and self-cleaning," Nano Lett. **10**(6), 1979–1984 (2010).
20. E. Garnett and P. Yang, "Light trapping in silicon nanowire solar cells," Nano Lett. **10**(3), 1082–1087 (2010).
21. J. Kim, A. J. Hong, J.-W. Nah, B. Shin, F. M. Ross, and D. K. Sadana, "Three-dimensional a-Si:H solar cells on glass nanocone arrays patterned by self-assembled Sn nanospheres," ACS Nano **6**(1), 265–271 (2012).
22. W.-C. Tan, J. R. Sambles, and T. Preist, "Double-period zero-order metal gratings as effective selective absorbers," Phys. Rev. B **61**(19), 13177–13182 (2000).
23. T. Khaleque, H. G. Svavarsson, and R. Magnusson, "Fabrication of resonant patterns using thermal nano-imprint lithography for thin-film photovoltaic applications," Opt. Express **21**(S4 Suppl 4), A631–A641 (2013).
24. J. Homola, S. S. Yee, and G. Gauglitz, "Surface plasmon resonance sensors: review," Sens. Actuators B Chem. **54**(1-2), 3–15 (1999).
25. F. Garcia-Vidal and L. Martin-Moreno, "Transmission and focusing of light in one-dimensional periodically nanostructured metals," Phys. Rev. B **66**(15), 155412 (2002).
26. A. Hessel and A. A. Oliner, "A new theory of Wood's anomalies on optical gratings," Appl. Opt. **4**(10), 1275–1297 (1965).
27. R. C. McPhedran and D. Maystre, "A detailed theoretical study of the anomalies of a sinusoidal diffraction grating," Opt. Acta (Lond.) **21**(5), 413–421 (1974).
28. T. Weiss, N. A. Gippius, G. Granet, S. G. Tikhodeev, R. Taubert, L. Fu, H. Schweizer, and H. Giessen, "Strong resonant mode coupling of Fabry–Perot and grating resonances in stacked two-layer systems," Photon. Nanostructures **9**(4), 390–397 (2011).
29. T. Li, J. Q. Li, F. M. Wang, Q. J. Wang, H. Liu, S. N. Zhu, and Y. Y. Zhu, "Exploring magnetic plasmon polaritons in optical transmission through hole arrays perforated in trilayer structures," Appl. Phys. Lett. **90**(25), 251112 (2007).
30. I. Botten, M. Craig, R. McPhedran, J. Adams, and J. Andrewartha, "The dielectric lamellar diffraction grating," J. Mod. Opt. **28**, 413–428 (1981).
31. M. G. Moharam, E. B. Grann, D. A. Pommet, and T. K. Gaylord, "Formulation for stable and efficient implementation of the rigorous coupled-wave analysis of binary gratings," J. Opt. Soc. Am. A **12**(5), 1068–1076 (1995).
32. L. Li, "Use of Fourier series in the analysis of discontinuous periodic structures," J. Opt. Soc. Am. A **13**(9), 1870–1876 (1996).
33. P. Lalanne and G. M. Morris, "Highly improved convergence of the coupled-wave method for TM polarization," J. Opt. Soc. Am. A **13**(4), 779–784 (1996).
34. M. A. Green, "Self-consistent optical parameters of intrinsic silicon at 300K including temperature coefficients," Sol. Energ. Mat. Sol. **92**(11), 1305–1310 (2008).
35. American Society for Testing and Materials, "ASTM G173-03 reference spectra," (2013), *http://rredc.nrel.gov/solar/spectra/am1.5/ASTMG173/ASTMG173.html*.
36. Z. M. Zhang, *Nano/Microscale Heat Transfer* (McGraw-Hill, 2007).
37. A. A. Tseng, K. Chen, C. D. Chen, and K. J. Ma, "Electron beam lithography in nanoscale fabrication: recent development," IEEE Trans. Electron. Packag. Manuf. **26**(2), 141–149 (2003).
38. M. Shinji and O. Yukinori, "Focused ion beam applications to solid state devices," Nanotechnology **7**(3), 247–258 (1996).
39. L. J. Guo, "Nanoimprint lithography: methods and material requirements," Adv. Mater. **19**(4), 495–513 (2007).
40. D. C. Skigin and R. A. Depine, "Transmission resonances of metallic compound gratings with subwavelength slits," Phys. Rev. Lett. **95**(21), 217402 (2005).
41. D. Xiang, L.-L. Wang, X.-F. Li, L. Wang, X. Zhai, Z.-H. Liu, and W.-W. Zhao, "Transmission resonances of compound metallic gratings with two subwavelength slits in each period," Opt. Express **19**(3), 2187–2192 (2011).
42. N. Nguyen-Huu and Y.-L. Lo, "Tailoring the optical transmission spectra of double-layered compound metallic gratings," IEEE Photon. J **5**(1), 2700108 (2013).
43. Y. J. Shin, C. Pina-Hernandez, Y.-K. Wu, J. G. Ok, and L. J. Guo, "Facile route of flexible wire grid polarizer fabrication by angled-evaporations of aluminum on two sidewalls of an imprinted nanograting," Nanotechnology **23**(34), 344018 (2012).

#195307 - $15.00 USD Received 5 Aug 2013; revised 22 Oct 2013; accepted 25 Nov 2013; published 4 Dec 2013

44. C.-L. Wu, C.-K. Sung, P.-H. Yao, and C.-H. Chen, "Sub-15 nm linewidth gratings using roll-to-roll nanoimprinting and plasma trimming to fabricate flexible wire-grid polarizers with low colour shift," Nanotechnology **24**(26), 265301 (2013).
45. B. Maes, J. Petráček, S. Burger, P. Kwiecien, J. Luksch, and I. Richter, "Simulations of high-Q optical nanocavities with a gradual 1D bandgap," Opt. Express **21**(6), 6794–6806 (2013).

1. Introduction

Tailoring absorption spectra of absorbers or emitters based on micro- and nanostructures with their geometric shapes plays a vital role in such various applications as energy conversion systems [1–9]. One of the important practical applications is solar cells; they have attracted much attention of researchers because of their ability to convert solar energy directly into electricity, which makes them attractive as alternative green energy sources. With a development of the micro- and nanofabrication technologies, solar energy absorbers based on one, two, and three dimensional (1,2,3D) grating structures have been promising candidates due to their performance improvements [10–21]. For example, 1D multi-layered grating structures comprising periodic arrays of rectangular [11–14, 18], triangular [10, 11, 14], sinusoidal [22], and complex or shifted slits [13, 15] were used to enhance absorptance of solar energy absorbers via grating coupling. Along with 1D structures, 2D gratings with different structured profiles, including square lattices of identical or different geometric holes on one and two sides of the gratings [16–18], or rectangular blocks [23], were also investigated. Meanwhile, 3D nanodome-, nanocone-, and nanorod-shaped structures have clearly demonstrated their improvement in enhancing optical absorption for solar cells [19–21].

Although the use of grating structures discussed above is to achieve the maximum light absorption for photovoltaic devices, such gratings have a complicated geometry and multiple layers; as a result, the fabrication process requires more material and equipment. Additionally, most of the studies were based on a variety of physical mechanisms found in nanostructures (e.g., surface plasmon polaritons, cavity resonance or Fabry-Perot resonance, Rayleigh-Wood anomaly, and magnetic polaritons [24–29]) in order to excite resonance wavelength ranges of interest in which the incoming light needs to be absorbed. Only a few studies have been reported on investigations of practical designs of absorbing structures that would be suitable for available fabrication techniques. Fabricated 2D and 3D structures have provided the solutions for the enhancement of light absorptance but they are not easily manufactured compared with 1D structures. Accordingly, 1D grating structures made of a single material are much preferred since they have an easily-fabricated geometry as well as offer acceptable performance. Therefore, a requirement for tuning the absorptance spectrum of 1D structures such that are feasibly manufactured with existing technologies is very important and thus addressed here.

Accordingly, the present study proposes a simple SGS as a solar energy absorber comprising an Si grating layer on top of an Si substrate. The optical performance of the CSG at wavelengths in the range of 300 to 1100 nm with incident transverse magnetic (TM) light is optimized by tuning the geometry parameters such that it is feasible to fabricate. The optimization employs an aspect ratio d/w (i.e., $0 < d/w < 1.0$). The first stage of the design is to preliminarily narrow down dimension ranges of the grating thickness (d) and the lamella width (w) via finding the aspect ratio for a region of maximum absorbed light. The next stage is to finely tune the lamella widths and add more Si within the grating period to enhance absorbed light via grating coupling. At this stage, some new structures feasible to manufacture, namely, simple gratings and compound gratings were analyzed and compared in terms of their optical performance. Note that the compound gratings have their surface profiles comprising two or more 1D simple grating profiles. In implementing the numerical analysis, the Rigorous Coupled-Wave Analysis (RCWA) method [30–33] was used to calculate the absorptance spectra of the gratings while the Finite Element Method (FEM-based COMSOL Multiphysics) is used to plot the magnetic field, energy density, and Poynting vector patterns within the grating structures to demonstrate the absorptance

#195307 - $15.00 USD Received 5 Aug 2013; revised 22 Oct 2013; accepted 25 Nov 2013; published 4 Dec 2013

enhancement. In general, it is shown that the CSG exhibits a very high absorptance over a wide wavelength range and is insensitive to angles of incidence.

2. Model development and numerical methods

2.1 Solar energy absorber structure and its material

Figure 1(a) shows a schematic illustration of the grating structure analyzed in this study. The structure consists of a rectangular Si grating on top of an Si substrate with a thickness of 500 μm. Using a simple profile and single material for the grating and substrate results in a cost-effective and straightforward fabrication process compared to that of 2D and 3D structures. As shown in Fig. 1(a), the geometry of the grating structure is defined by the period (Λ), the lamella width (w), and the grating thickness (d). In the present analysis, the incident light including TM or transverse electric (TE) waves travels through free space with an orientation defined by the polar angle θ between the wavevector **k** and the surface normal **z**. Note that **H** and **E** denote oscillation directions of magnetic and electric fields, respectively.

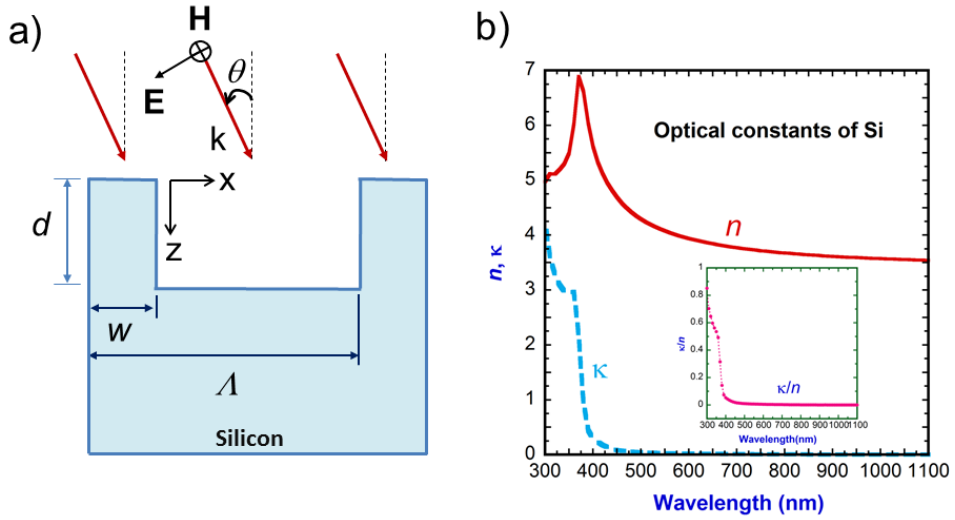

Fig. 1. (a) Schematic illustration of the grating structure whose geometry is defined by the grating period Λ, the grating thickness d and the lamella width w. The transverse magnetic wave (**H**) (parallel to the grating grooves or y-axis) is incident on the grating with a wavevector **k** and an angle θ. (b) Optical constants of the Si material used in this study [34]; the inset figure shows the index ratio (κ/n) between the extinction index κ and the refractive index n.

In analyzing the absorptance spectra of the grating structure shown in Fig. 1(a), the wavelength-dependent dielectric function, $\varepsilon_\lambda = (n + i\kappa)^2$, of Si is obtained from Ref [34]. using a linear interpolation between two neighboring data of the extinction index κ and the refractive index n. Figure 1(b) shows spectra of κ and n in the wavelength range of 300 and 1100 nm applicable to harvesting solar energy because the solar energy irradiating on the ground corresponds to wavelengths of 295 ~2500 nm [35]. The inset in Fig. 1(b) shows the index ratio (κ/n) which can characterize the relation between the optical property and absorptance feature (A) of the plain Si with a thickness of 500 μm. For normal incidence, A of plain Si can be calculated as [36]:

$$A = \frac{4n}{(n+1)^2 + \kappa^2} = \frac{4(\kappa/n)^{-1}}{\kappa\left[\kappa(\kappa/n)\right]^2 + \kappa} \tag{1}$$

As shown in the inset, the ratio κ/n is large at short wavelengths ($300 < \lambda < 370$ nm) and then decreases quickly; and accordingly, A becomes significant at long wavelengths because

#195307 - $15.00 USD Received 5 Aug 2013; revised 22 Oct 2013; accepted 25 Nov 2013; published 4 Dec 2013

both κ and n decrease (see Eq. (1) above). Therefore, Si is selected for simulations here due to its high refractive index and low losses properties that are suitable for solar cells; moreover, Si is also easy to integrate with other optoelectronic devices.

2.2 Design guidelines and numerical methods

In designing the subwavelength grating structure for solar energy absorbers shown in Fig. 1, the parameter of interest is the aspect ratio (d/w) of the grating thickness (d) and the lamella width (w). The aspect ratio was set in the range of 0 ~1 for the purpose of being able to use available fabrication facilities [37–39] (e.g., electron-beam lithography, focused ion beam lithography, nanoimprint lithography, etc.). Moreover, this assumption also reduces many degrees of freedom for calculations. The lamella width w related to the filling factor ($0 < f < 1$) and the grating period (Λ) is defined by $w = f\Lambda$. To be specific, the designed parameters were sought for optimization based on subwavelength gratings which are widely used for many applications of optoelectronic devices [3, 40, 41]. For example, the grating period was set as Λ = 300 nm due to $\Lambda \le \lambda_{min}$, i.e., the period of the grating is smaller than the wavelength of the incoming light in a wavelength range of 300 ~1100 nm. The SG was selected in the present study because of its unique property in generating only 0th diffraction when interacting with incident light. Accordingly, the lamella width w could be specified as $0 < w < 300$ nm. Finally, the grating thickness (d) was determined by the thickness-to-lamella width ratio as $0 < d < 300$ nm.

In this study, the geometry of the SGS was optimized using the RCWA [30–33] to calculate the absorptance spectrum based on the specified parameters of the grating thickness and the lamella width with the wavelength range of 300 ~1100 nm. After the optimized geometric parameters of the SGS were defined, its structured profiles were tuned to find the new structure exhibiting the best performance while preserving its manufactured geometry. In the simulation, the calculated absorptance spectrum (A) was obtained indirectly from the reflectance R, i.e., $A = 1\text{-}R$ [3, 9]. Additionally, to investigate the enhancement of absorptance obtained from the optimized grating structure, the TM field, energy density, and Poynting vector distributions within the SGS were analyzed using the FEM method (COMSOL Multiphysics). To ensure the accuracy of the numerical results, the FEM method was implemented using a 2D model with a mesh size based on the relation $\Delta = \lambda/10$ where λ is the wavelength of incident light. In addition, the boundary condition in the z-direction was selected as the perfectly matched layer while the periodic boundary condition was applied in the x-direction. Based on these conditions, the calculated absorptance of grating structures within one and ten periods was verified with both results being identical. Note that the FEM was used to obtain the distributions of magnetic field, energy density, and Poynting vectors within the SGS after all geometric parameters were verified by the RCWA method. The numerical results obtained from both methods were also validated before calculations.

3. Results and discussion

3.1 Absorptance of designed SGS

Figure 2 shows the absorptance contour plots of the SGS with Λ = 300 nm and a range of the selected parameters based on the aspect ratio d/w (e.g., $20 < d < 200$ nm and $0 < w < 300$ nm) and the wavelengths in the range of 300 ~1100 nm for the TM wave at normal incidence. Examining Fig. 2 shows that the TM wave absorptance at the grating thickness d = 20 nm and 40 nm is smaller than those of the structures with $d > 40$ nm in a wide range of wavelengths and lamella widths. At the grating thickness of 80 nm, the maximum absorptance marked by white occurs at two regions of the lamellae widths (i.e., $30 < w_1 < 130$ nm and $120 < w_2 < 250$ nm), while the left ones have one zone at the range w of 30 ~250 nm. Moreover, it is seen that the absorptance of the structures with grating thicknesses d = 120 and 160 nm is maximum at a wide wavelength range of 600 ~1100 nm and the lamella width of 50 ~250 nm compared with those of the other structures. Overall, the results presented in Fig. 2 show that the optimized simple SGSs achieve a maximum absorptance with the grating thickness $d \ge 80$ nm

#195307 - $15.00 USD Received 5 Aug 2013; revised 22 Oct 2013; accepted 25 Nov 2013; published 4 Dec 2013

and the lamella width $50 < w < 250$, and their absorptance spectra are not covered by the whole wavelength range of interest.

3.2 Tuning geometric profiles of the designed structure

Previous studies have shown that compound gratings (CGs) whose profiles are a superposition of two or more 1D simple grating features are promising candidates for controlling optical transmission [40–42]. Accordingly, in this study the simple grating structure's geometry was modified to build CGs with different profiles as shown in Fig. 3, in order to tailor absorptance spectra. Importantly, controlling structured profiles of the CGs is to follow the aspect ratio for ease of fabrication. From inspection of Fig. 2, one can see that the absorptance spectra of the simple grating structures with grating thicknesses d = 80, 120, 160, and 200 nm and lamella widths w = 150 ~200 nm are maximum but do not extend over the whole range of wavelengths of interest. For example, the grating structures with d = 80, 120 and 160 nm and w = 150 ~200 nm exhibit low absorptance of about 0.45 at wavelengths of 300 ~400 nm while the one with d = 200 nm displays very high or low absorptance in a short range of wavelengths. However, the grating with d = 80 nm and w = 60 and 120 nm gives high absorptance of 0.75 ~0.85 in the whole wavelength region. Thus, we select this grating structure since it offers good performance in the wide range of wavelengths, i.e., 300 ~1100 nm to construct CGSs in order to enhance the absorptance. The geometric parameters of the constructed grating are also compatible with current fabrication techniques (e.g, electron beam lithography, nanoimprint lithography, ect.). Among the available techniques, nanoimprint lithography is considered as a promising method due to the reasons. It can be used to fabricate nanograting structures with critical dimensions of lamella widths from 15 to 70 nm, and it has been developing to a roll-to-roll processing method which can be applied to manufacture nanodevices over large areas [39, 43, 44]. In addition, the selected lamella widths are much smaller than that of the grating period Λ; as a result, there is room for tailoring the structured profiles based on d/w. Following schematic illustrations shown in Fig. 3 are the new structures constructed based on the selected geometric parameters.

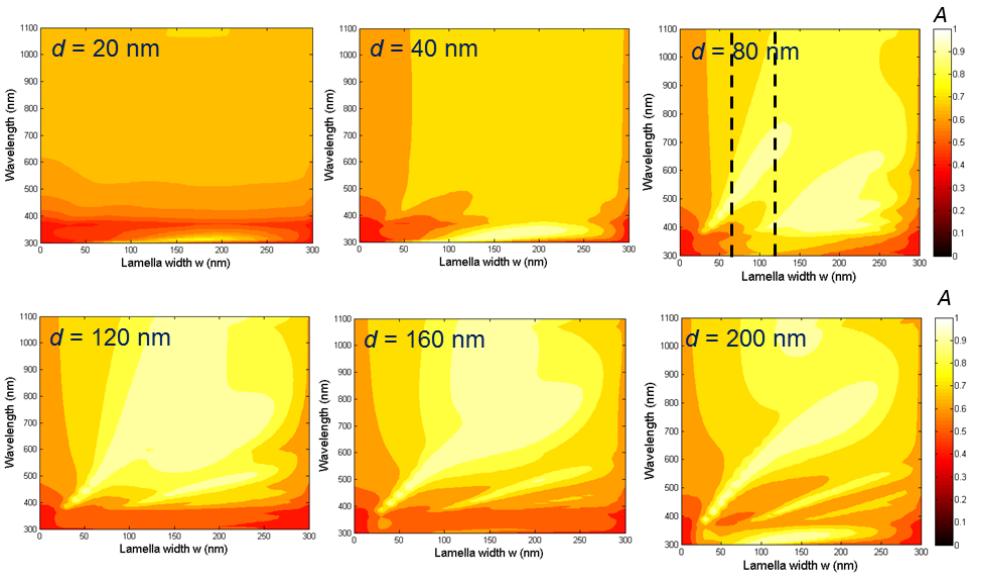

Fig. 2. Contour plots of absorptance (A) for wavelengths of 300 ~1100 nm at TM normal incidence with variations of the grating thickness, $20 < d < 200$ nm, and the lamella width, $0 < w < 300$ nm. The designed parameters for tuning geometric structures to enhance absorptance are marked by two dash lines.

Figure 3 presents a schematic illustration of newly built structures classified by group I and II with the same grating period (Λ = 300 nm) and the grating thickness (d = 80 nm). The

#195307 - $15.00 USD Received 5 Aug 2013; revised 22 Oct 2013; accepted 25 Nov 2013; published 4 Dec 2013

group I comprises a simple grating I (SGI) and a compound grating I (CGI) with the same parameters, but CGI has two identical lamella widths in each period (w_1 = 60 nm). The group II consists of a SGII with w_2 = 120 nm and a CGII with different w (w_1 = 60 nm and w_2 = 120 nm). Note that the simple grating with d = 80 nm and w = 60 and 120 nm was chosen to build these compound gratings due to their advantages as analyzed above. With these geometric parameters of the grating, we take the maximum w of 120 nm and minimum w of 60 nm to build two types of SGs with the same thickness d, e.g., SGI and SGII. Then, we manipulate the grating structure by adding more Si lamella materials to become CGI and CGII with d = 80 nm, w_1 = 60 nm, and w_2 = 60 nm. The distances between two Si lamellae w_1 and between w_1 and w_2 are all equal to w_1 as shown in Fig. 3. It is also noted that the analysis for these structures is considered having the same coordinate system as that shown in Fig. 1, with TM (TE) waves being incident on the grating surface, whose magnetic field **H** (**E**) component is parallel to the slits.

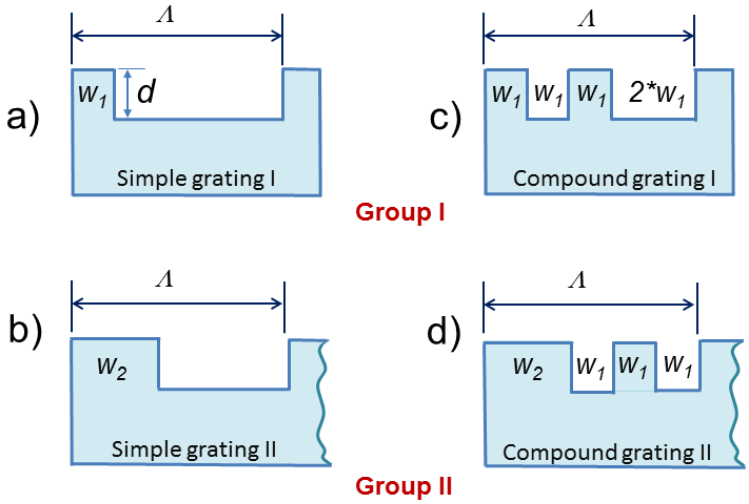

Fig. 3. Schematic of simple and compound grating structures with the grating period Λ, the lamella widths (w_1 = 60 nm and w_2 = 120 nm), and the same grating thickness (d = 80 nm). The proposed structures are classified by groups I and II (TM wave incidence in all cases).

Figure 4 shows the absorptance spectra of simple and compound grating structures at TM normal incidence with wavelengths ranging from 300 ~1100 nm. Note that the absorptance spectrum of the plane Si is also shown for comparison. Note also that the left-hand side inset shows the TE wave absorptance while the right-hand side inset shows a comparison of spectral absorptance peak with angles of incidence between the RCWA and FEM methods. As shown in Fig. 4, the results obtained from the grating structures of group II are better than those of group I. For example, the average absorptance of SGII is 84% while that of SGI is only 74%, and the average absorptance of CGII is 92% with CGI having only 83%. However, the performance of the grating structures is significantly higher than that of the plain Si with its absorptance of 60%. The absorptance spectra of the plain Si was calculated using Eq. (1) and is marked by the red solid line in the left-hand side of Fig. 4. This result matches well with that obtained from RCWA codes (marked by the dash line).

#195307 - $15.00 USD Received 5 Aug 2013; revised 22 Oct 2013; accepted 25 Nov 2013; published 4 Dec 2013

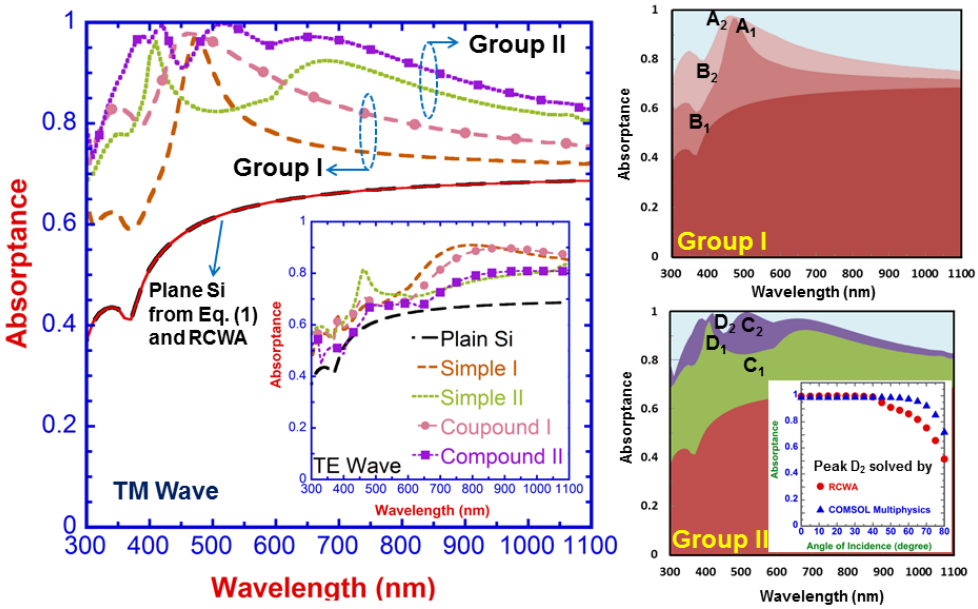

Fig. 4. Absorptance spectra of simple and compound grating structures (group I and II) for the TM wave at normal incidence. The left-hand side inset represents the absorptance spectra plotted for TE wave, while the right-hand side inset shows validation between the RCWA and FEM methods used to calculate spectral absorptance peak D_2 (located a λ = 420 nm) with different angles of incidence.

One can see from inspecting Fig. 4 that the TM absorptance peaks and valleys of SGI and CGI at angle of $\theta = 0°$ are equal to 0.97 (A_1, λ = 470 nm) and 0.59 (B_1, λ = 370 nm), and 0.98 (A_2, λ = 460 nm) and 0.78 (B_2, λ = 390 nm), respectively. Moreover, it is observed that CGI achieves higher absorptance over a larger wavelength range, as clearly shown in the top right-hand side of Fig. 4. The absorptance of SGI is much enhanced when adding one lamella width in each grating period, called CGI. As it is seen, the peak A_1 and the valley B_1 become A_2 and B_2. Similarly, CGII exhibits absorptance higher than not only SGII but also all gratings group I over a wide range of wavelengths by increasing one of lamella widths to a double (w_2 = 120 nm). For example, the peak C_1 (located at λ = 515 nm) and the valley D_1 (located at λ = 410 nm) rise up to C_2 (located at λ = 515 nm) and D_2 (located at λ = 420 nm) when the grating geometry is modified. Interestingly, the valley C_1 increases to become a maximum–the peak D_2; as a result, CGII absorbs more energy at this peak wavelength, as shown in the bottom right-hand side of Fig. 4. In general, the results illustrated in Fig. 4 show that CG structures exhibits higher energy than SG ones.

In addition, the bottom right-hand side inset in Fig. 4 shows a comparison between using the RCWA and FEM methods to calculate the absorptance peak D_1 versus angles of incidence, as an example. It is seen that the results obtained from the two methods are well-matched at angles of incidence between 0 ~45° as illustrated by filled triangle and circle markers. For incident angles greater than 45°, both methods are not in a good agreement due to numerical errors influenced by boundary conditions (perfectly matched layers) in the FEM method [45]. Thus, with a large range of incident angles it is simply sufficient to investigate the enhanced light trapping in the grating structures using the FEM method. Overall, Fig. 4 shows that the subwavelength grating structure has a potential application for solar energy absorbers due to its better performance achieved by controlling its geometric profiles via a modification of the grating lamella within each period. For example, the results presented in Fig. 4 demonstrate that the CGII may be used as the best solution for solar energy absorber with an average absorptance of 92% among the others.

#195307 - $15.00 USD Received 5 Aug 2013; revised 22 Oct 2013; accepted 25 Nov 2013; published 4 Dec 2013

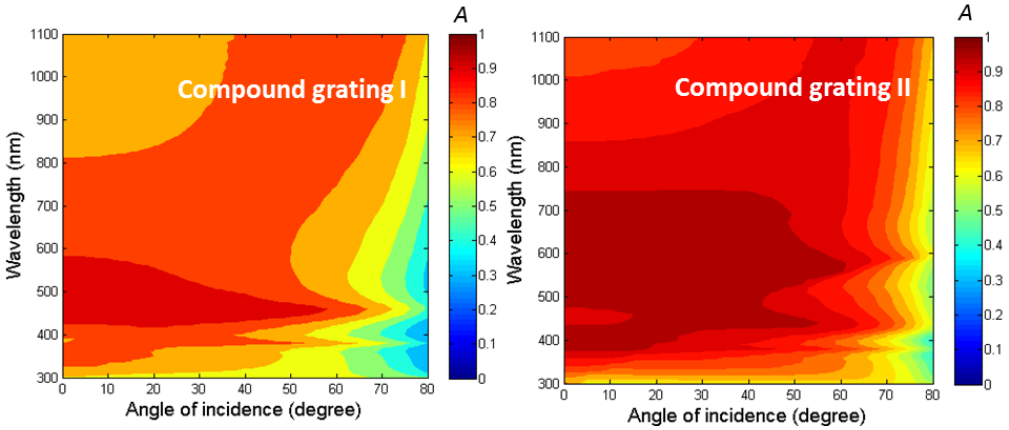

Fig. 5. Absorptance for wavelengths of 300 ~1100 nm at the TM wave versus angles of incidence for CGI and CGII structures.

Figure 5 shows the absorptance contour plots for wavelengths of 300 ~1100 nm at TM incidence for CGI and CGII as it depends on incident angles of 0 ~80°. It is observed that the absorptance of CGI is greater at wavelengths ranging from 300 ~800 nm corresponding to incident angles ranging from 0 ~60°. Meanwhile, CGII exhibits very high absorptance, around 100%, in a large range of wavelengths and angles of incidence, i.e., $300 < \lambda < 1100$ nm and $0 < \theta < 75°$, respectively. Moreover, it is also seen that CGII absorbs maximum energy at a large range of wavelengths (400 ~750 nm) and of incident angles (0 ~60°) compared with CGI. Overall, the results presented in Fig. 5 suggest that the CGII works as a solar energy absorber possessing the highest absorptance over the whole wavelength range with its absorptance spectrum being quite insensitive to the angle of incidence compared with other studied grating structures.

3.3 Magnetic fields, energy density, and Poynting vectors

Figure 6 shows magnetic fields (top), the time-average Poynting vector, and the energy density (bottom) at points A_1, A_2, B_1, and B_2, within one grating periods of a structure in group I, obtained from the FEM method-based COMSOL Multiphysics. The background contour of the top figures is the *y*-component intensity of magnetic fields while that of the bottom figures is the time-average energy density. The arrows indicate the Poynting vectors representing the energy flow rate and the direction. It can be seen from Fig. 6 that the magnetic fields at peaks A_1 at $\lambda = 470$ nm and A_2 at $\lambda = 460$ nm are confined in the lamella width regions (as illustrated by white) much more than those at valleys B_1 at $\lambda = 370$ nm and B_2 at $\lambda = 390$ nm. It suggests that there is a significant light trapping effect inside these structures. Moreover, the incident energy trapping in the grating structures is at the same positions along with the enhanced magnetic fields as shown in the plots of the energy density and the Poynting vector distributions. To be specific, the energy density of CGI concentrates much under the lamella areas when compared with that of SGI. Meanwhile, the Poynting vectors of CGI at the grating inlets are guided and trapped in the lamella corners and substrate much more than that of SGI. Thus, the total energy is collected in CGI. Overall, these plots demonstrate that the enhancement of magnetic fields excited in the grating structures illustrates the coupling of the grating and incident light or Fabry Perot resonance.

#195307 - $15.00 USD Received 5 Aug 2013; revised 22 Oct 2013; accepted 25 Nov 2013; published 4 Dec 2013

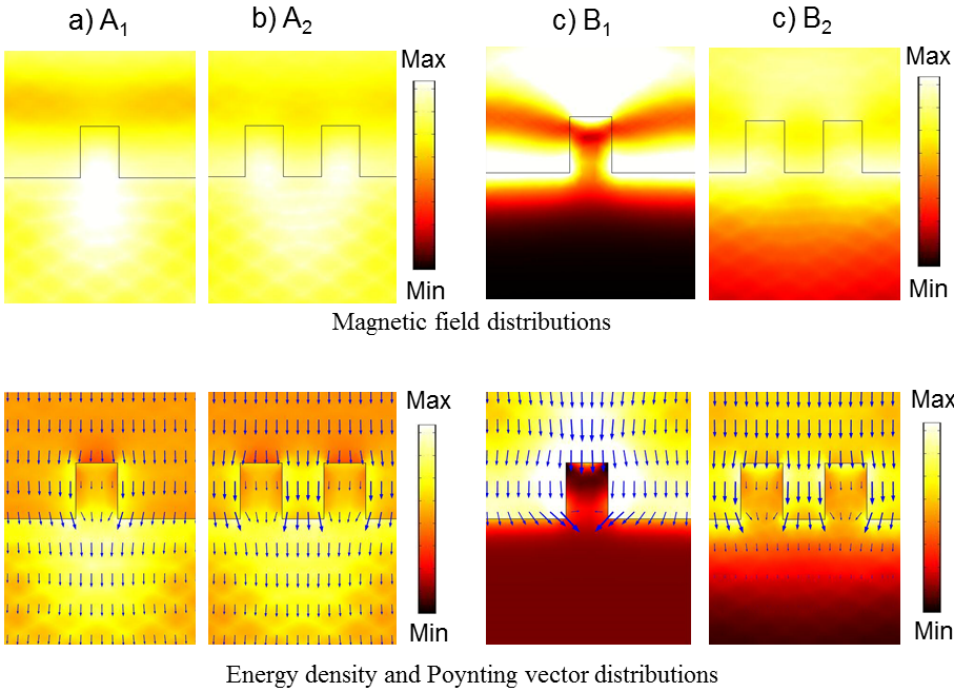

Fig. 6. Near-field patterns of grating structures of group I including SGI and CGI at points A_1 (at λ = 470 nm), A_2 (at λ = 460 nm), B_1 (at λ = 370 nm), and B_2 (at λ = 390 nm) as plotted in the top right-hand side of Fig. 4. The top figures represent electromagnetic field distributions while the bottom figures show energy density and Poynting vector patterns within one grating period.

Similar to Fig. 6, Fig. 7 shows magnetic fields (top), the time-average Poynting vector, and the energy density (bottom) of the structure group II at points C_1 located at λ = 515 nm, C_2 located at λ = 515 nm, D_1 located at λ = 410 nm, and D_2 located at λ = 420 nm. In Fig. 7, the background contour of the top figures is the *y*-component of the intensity of magnetic fields, while that of the bottom figures is the time-average energy density. The Poynting vectors representing the energy flow rate and the direction are indicated by arrows at the bottom figures. One can see by inspecting Fig. 6 that the magnetic fields at all points are concentrated under the lamella regions (as illustrated by white). Additionally, the energy is much confined in CGII due to having more grating lamella and is also at the same positions as the enhanced magnetic fields. As a result, the energy is collected by CGII much more than that by SGII, as the absorptance spectra and energy density distributions show in Fig. 4 and the bottom plots of Fig. 7, respectively. For example, it is clearly seen that at the valley C_1 and the peak D_1, the incident energy absorbed by SGII is smaller than at peaks C_2 and D_2 in CGII, as demonstrated by the depth of the energy density penetrating into the structure. Thus the results presented in Fig. 7 suggest that CGII absorbs most of solar energy with an average absorptance of 92% compared with that of the other structures due to the excitation of Fabry-Perot effect in which the magnetic fields strongly couple with grating lamellae.

#195307 - $15.00 USD Received 5 Aug 2013; revised 22 Oct 2013; accepted 25 Nov 2013; published 4 Dec 2013

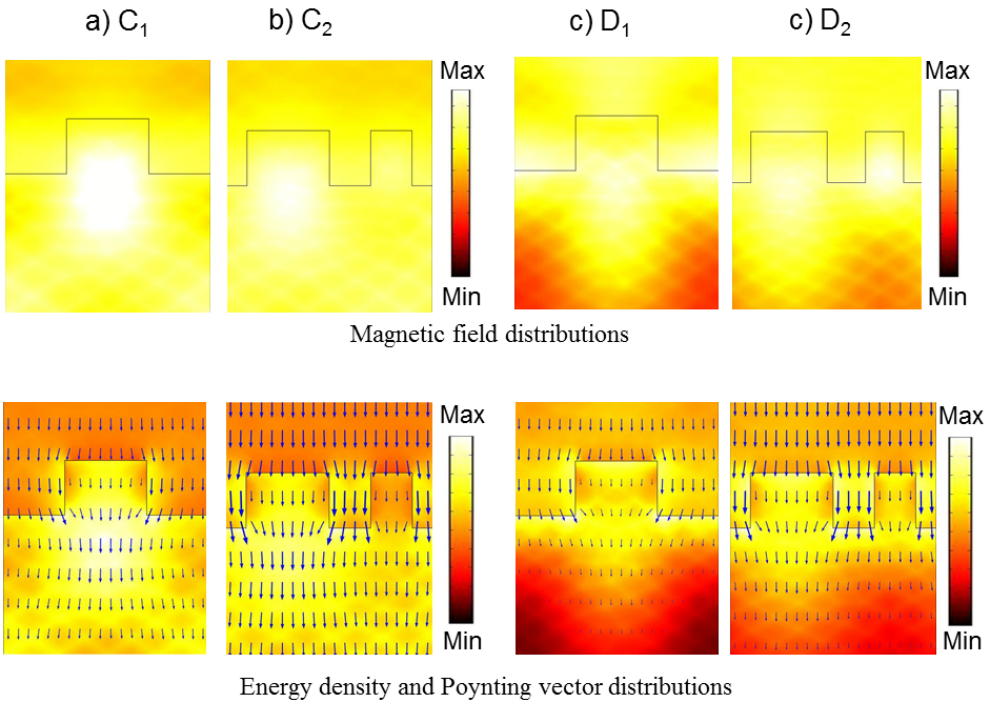

Fig. 7. Near-field patterns of grating structures of group II including SGII and CGII at points C_1 (at $\lambda = 515$ nm), C_2 (at $\lambda = 515$ nm), D_1 (at $\lambda = 410$ nm), and D_2 (at $\lambda = 420$ nm) as plotted in the bottom right-hand side of Fig. 4. The top figures represent electromagnetic field distributions while the bottom figures show energy density and Poynting vector patterns within one grating period.

4. Conclusions

This study has proposed an applicable method for designing solar energy absorbers based on the experimental rules using the RCWA method and the FEM-based COMSOL Multiphysics. The applied fabrication rules are based on the aspect ratio of the grating thickness and grating lamella width, which may be implemented using many fabrication facilities. The RCWA method was used to calculate the absorptance of the grating structures at wavelengths in the range of 300 nm $\leq \lambda \leq$ 1100 nm while the FEM method was applied to compute the magnetic field, energy density, and Poynting vector distributions. The results have shown that the compound grating type II yields the highest absorptance of 92%, which is significantly higher, about 1.5 times, than that of the conventional gratings and the plain Si. Additionally, the absorptance spectrum of the proposed grating is insensitive to the angle of incidence of the incoming light. In general, the results presented in this study confirm the effectiveness of the proposed method providing various solutions in designing optoelectronic devices. For instance, some simple grating structures as shown in Fig. 2 may be used to design narrow-band thermal emitters/absorbers or biosensors. On the other hand, compound grating structures are best suitable for broad-band thermal emitters/absorbers or other energy harvesting applications.

Acknowledgments

The authors gratefully acknowledge the financial support provided to this study by ASPIRE (Applied Science in Photonics and Innovative Research in Engineering,) NSERC (Natural Sciences and Engineering Council,) CREATE (Collaborative Research and Training Experience program) program of Canada; and by the Operational Program Education for Competiveness, the European Social Fund, and the state budget of the Czech Republic with

#195307 - $15.00 USD Received 5 Aug 2013; revised 22 Oct 2013; accepted 25 Nov 2013; published 4 Dec 2013

the project named Opportunity for young researchers reg No. #CZ.1.07/2.3.00/30.0016, the Regional Centre of Excellence RMTVC project No. #CZ.1.05/2.1.00/01.0040, and the Grant Agency of the Czech Republic No. #P205/11/2137. Dr. Nghia also wishes to thank Profs. Y.-L. Lo and Y.-B. Chen (National Cheng Kung University, Taiwan) for useful discussions on the RCWA method.

#195307 - $15.00 USD Received 5 Aug 2013; revised 22 Oct 2013; accepted 25 Nov 2013; published 4 Dec 2013